Supporting Information for

A facile approach for synthesizing nitrogen-doped carbon supported circular trough-shaped FeCo alloy-based electrocatalysts for oxygen reduction reaction

Kun Yang,[a] Jing Liu,[a,] Bin Li,[a] Zhicheng Xu,[a] Xiang Ji,[a] Xinchun Yang,[b,*] Jianping Long[a,*]*

[a]College of Materials and Chemistry & Chemical Engineering, Chengdu University of Technology, 1#, Dongsanlu, Erxianqiao, Chengdu 610059, Sichuan, P. R. China

[b]Institute of Technology for Carbon Neutrality, Shenzhen Institutes of Advanced Technology, Chinese Academy of Sciences, Shenzhen, 518055, P. R. China

*Corresponding Authors: E-mail: jingliu@cdut.edu.cn (Jing Liu), xc.yang@siat.ac.cn (Xinchun Yang), longjianping@cdut.cn (Jianping Long)

The file includes:

Part I. Supplementary Notes

Note S1 methods

Chemicals. Activated carbon support (Black Pearls 2000), anhydrous ferric chloride ($FeCl_3$, 98%), cobaltous oxide (CoO, 99.5%), and melamine ($C_3H_6N_6$, 99.5%) were provided by Beijing Innochem Science & Technology Co., Ltd. The Nafion PFSA polymer (5wt %) was supplied by DuPont. Potassium hydroxide (KOH, 85%) was provided by Sichuan Xilong Science and Technology Co., Ltd. Anhydrous ethanol (C_2H_5OH, 99.9%) and isopropanol ($(CH_3)_2CHOH$, 99.7%) were supplied by Chengdu Jinshan Chemical Reagent Co., Ltd. All chemicals used in this study were of analytical grade and were used as received without further purification.

Preparation of FeCo/NC: The FeCo/NC was prepared by a one-step mixed pyrolysis method. Firstly, 50 mg of BP-2000, 0.5g melamine, 0.728 mg of anhydrous ferric chloride and 4.138 mg of cobaltous oxide were respectively added into an agate jar and ball milled for 2.0 hours to obtained a black solid powder. Then, the powder was placed in an alumina crucible and heat-treated at 900 °C for 1 hour in a tube furnace under an argon atmosphere, with a heating rate of 5 °C min^{-1}, to obtain the final sample FeCo/NC. The influence of heat-treatment temperature on the structure and performance of FeCo alloy-based catalysts was studied by changing the pyrolysis temperature (800°C and 1000 °C). For comparison, Fe/NC and Co/NC were prepared under the same preparation conditions as FeCo/NC.

Material Characterization. Transmission Electron Microscopy (TEM) analyses were conducted on a JEOL JEM-F200 microscope, operating at an accelerating voltage of 200 kV, to investigate the structural and morphological characteristics of the samples comprising FeCo alloy. Both bright-field and dark-field images were acquired under varying imaging modalities. X-ray Photoelectron Spectroscopy (XPS) analyses were performed utilizing a Sigma Probe system (manufactured by Thermo VG Scientific), equipped with a micro-focused monochromator X-ray source. Inductively Coupled Plasma-Optical Emission Spectrometry (ICP-OES) measurements, employing the Agilent 720 spectrometer, were performed to ascertain the definitive loading concentrations of Fe and Co within the prepared samples. Following degassing of the samples at 100 °C, nitrogen (N_2) adsorption-desorption isotherms were measured at 77 Kelvin (K) using an ASAP2460 instrument from Micromeritics. Utilizing the data processed by the integral software of the ASAP2460, which incorporates the Brunauer-Emmett-Teller (BET) equation, the Barrett-Joyner-Halenda (BJH) model, and density functional theory (DFT) approaches, the specific surface area, the distribution of mesopore sizes, and the distribution of micropore sizes within the catalytic material were accurately determined, respectively. X-ray diffraction (XRD) tests were carried out on a SmartLab X-ray diffractometer (RIGAKU, Cu Kα radiation, $\lambda = 0.15418$ nm). The Raman spectrum was obtained on a laser confocal Raman spectroscopy (Labram–010, Horiba–JY) employing the Nd: YAG laser wavelength of 633 nm.

Electrochemical measurement. The well-known three-electrode system was adopted to estimate the electrocatalytic ORR activity of the FeCo alloy-based catalysts at 25 °C. A 5-millimeter diameter glassy carbon (GC) rotating disk electrode was prepared by depositing catalyst inks onto its surface to serve as the working electrode for subsequent electrochemical testing. In a typical protocol, 5 mg of FeCo alloy-based catalyst powder was uniformly dispersed into a solution mixture comprising 960 μL of isopropanol and 40 μL of a 5 wt % Nafion solution, with continuous ultrasonication applied for a duration of 30 minutes to facilitate the formation of catalyst ink. Subsequently, 12μL of the catalyst ink were deposited onto the surface of the glassy carbon (GC) electrode to yield the modified working electrode. For comparison, an identical procedure was employed to decorate the working electrode with a commercially available carbon-supported platinum catalyst containing 20 weight wt% platinum on carbon (Pt/C, sourced from TKK). A mercury oxide electrode (Hg/HgO) was employed as the reference electrode, whereas a Pt mesh acted as the counter electrode. The EG&G (Model CHI760e) potentiostat/galvanostat system was used to monitor the electrode potential.

The electrocatalytic activity of all aforementioned catalysts towards the oxygen reduction reaction (ORR) was evaluated in an aqueous solution of 0.1 M KOH, saturated with O_2, at 25 °C. Linear scan voltammetry (LSV) measurements were conducted to acquire the polarization curves for the oxygen reduction reaction (ORR), within a potential range spanning from 0.005 to 1.2 V versus the reversible hydrogen electrode (RHE). These measurements were executed at a scan rate of 10 mV s^{-1} and a rotation speed of 1600 rpm. In order to clarify the long-term operation stability of FeCo/NC and commercial Pt/C, 10,000 potential cycles were conducted in a 0.1 M KOH solution with saturated O_2 at 25 °C (potential range: 0.5−1.1 V; scan rate: 100 mV s^{-1}). Based on the ORR polarization plots with different rotating speeds from 225 to 1600 rpm, the ORR path selectivity of FeCo/NC was first estimated using the Koutecky−Levich first-order equation (eq 1 and 2),[1,2]

$$\frac{1}{j} = \frac{1}{j_k} + \frac{1}{j_L} = \frac{1}{j_k} + \frac{1}{B\omega^{\frac{1}{2}}} \tag{1}$$

$$B = 0.62nFC_0D_o^{\frac{2}{3}}v^{-\frac{1}{6}} \tag{2}$$

Where j is the measured current density, which consists of kinetic (j_K) and diffusion-limiting current (j_L), B is a constant, ω is the rotation speed in rpm, F is the Faraday constant (96485 C mol^{-1}), n is the number of electrons transferred per oxygen molecule, C_0 is the bulk concentration of O_2 (1.26×10^{-6} mol cm^{-3} in 0.1 M KOH), D_0 is the diffusion coefficient for O_2 in 0.1 M KOH (1.93×10^{-5} cm^2 s^{-1}), and v is the kinetic viscosity of solution (0.01009 cm^2 s^{-1}).

Based on the ring current density (i_R) and disk current density (i_D)obtained from the

rotating ring-disk electrode (RRDE), the percentage of H_2O_2 yielded and electron transfer number from ORR are obtained to further verify the ORR path selectivity of FeCo/NC by following eqs 3 and 4, respectively,[3,4]

$$H_2O_2(\%) = \frac{200 \times \frac{I_R}{N}}{\frac{I_R}{N} + I_D} \quad (3)$$

$$n = \frac{4 \times I_D}{\frac{I_R}{N} + I_D} \quad (4)$$

Where I_D and I_R represent the disk current and ring current, respectively. N denotes the electrode's ring collection efficiency, determined to be 0.37.

In order to evaluate the methanol tolerance of the prepared catalyst, 1M methanol solution was injected into a 0.1M KOH electrolyte at a rotational speed of 1600 rpm to record the chrono-amperometric curve, which was kept at room temperature. Electrochemical impedance spectroscopy (EIS) tests were performed at 0.8 V (1600 rpm) in an O_2-saturated 0.1 M KOH electrolyte. The frequency range is 100 kHz to 100 MHz, and the voltage amplitude is 5 mV.

Zinc−Air Battery Measurements. For zinc-air battery (ZAB) testing, the synthesized catalyst was deposited onto carbon paper, serving as the air cathode electrode, with a certain catalyst loading. A refined zinc plate, possessing a thickness of 5 mm, was utilized as the anode, while a solution composed of 6 M KOH and 0.1 M $ZnSO_4 \cdot 7H_2O$ served as the electrolyte in the respective zinc-air battery (ZAB) setup. For comparison, a zinc-air battery (ZAB) featuring a commercial Pt/C cathode was additionally prepared. A Land battery test system (Wuhan LAND Electronics Co., Ltd.) was used for galvanostatic tests. The power density profiles of the battery were generated through the multiplication of instantaneously monitored voltage and current density values. The discharge and cycling performance of the battery were evaluated at a current density of 20 mA cm^{-2}. Prior to and following the discharge, the zinc electrode was cleaned using alcohol-soaked cotton and dried under ambient conditions. Additionally, the quantity of zinc consumed during the discharge process was meticulously monitored to determine the specific capacity of the battery.

Part II. Supplementary Figures

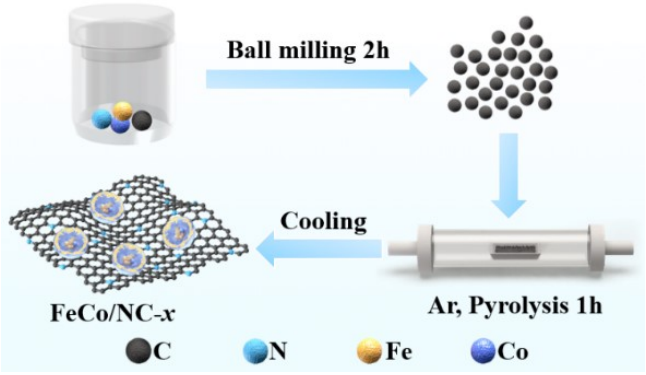

Fig.S1 Schematic illustration of the preparation process of FeCo/NC-*x* catalyst (*x* = 800, 900, 1000 °C).

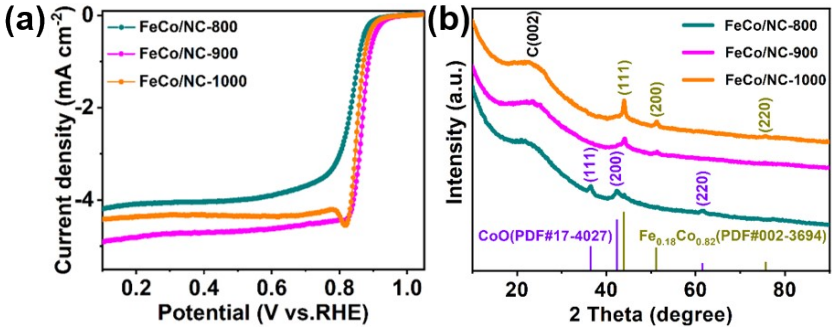

Fig. S2. (a) RDE polarization curves and (b) X-ray diffraction spectra of catalysts FeCo/NC-*x* (*x* = 800, 900, 1000 °C).

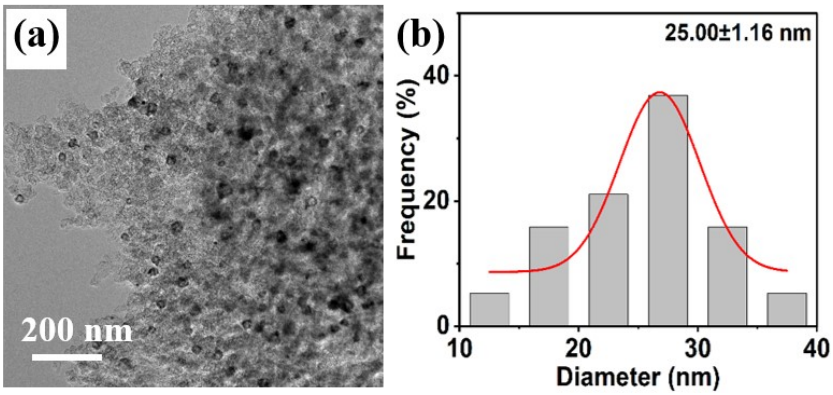

Fig. S3. (a) Low-magnification bright-field TEM images of different regions in FeCo/NC; (b) The size distribution of FeCo alloy nanoparticles in FeCo/NC.

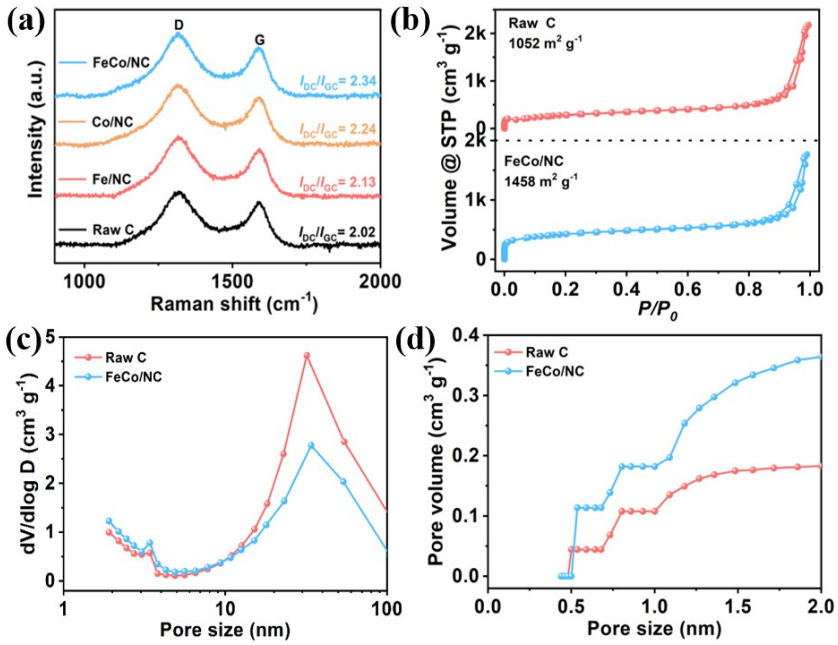

Fig.S4. Raman Spectra of raw C, Fe/NC, Co/NC and FeCo/NC; (b) N_2 adsorption/desorption isotherms of raw C and FeCo/NC; (c) The mesoporous size distribution of raw C and FeCo/NC; (d) the microporous volume (pore size < 2nm) of raw C and FeCo/NC.

The Raman Spectra (Fig.S4a) show that nitrogen-doped carbon-supported metal-based catalysts contain more defects than the raw active carbon (C). Additionally, FeCo/NC exhibits the highest I_{DC}/I_{GC} value, indicating that more defects can be generated during the alloy formation process, which have been shown to be beneficial for promoting the reaction kinetic of ORR.[5] Additionally, raw C and FeCo/NC show similar N_2

adsorption/desorption isotherms (Fig. S4b), but different mesoporous size distributions (Fig.S4c) and micropores size distributions (Fig. S4d). Due to the increase of defect generated during the alloy formation process (Fig.S4a), the number of mesopore with the size of about 33 nm decreased (Fig. S4c), while the microporous volume (pore size < 2 nm) of FeCo/NC increased (Fig. S4d), resulting in a larger BET surface area of FeCo/NC than raw C (Fig. S4b),[6] which is beneficial of facilitating the expose of more ORR active sites in the catalysts.[7]

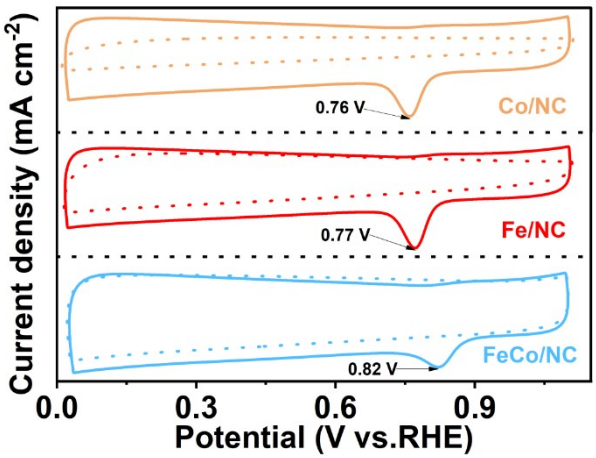

Fig.S5. CV curves of Co/NC, Fe/NC, and FeCo/NC in N_2-saturated (dashed line) and O_2-saturated (solid line) 0.1 M KOH electrolytes.

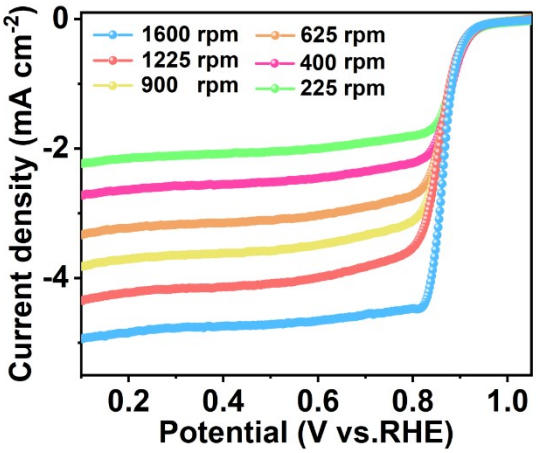

Fig.S6. LSV curves of FeCo/NC with different rotation rates at a scan rates of 10 mV s^{-1}.

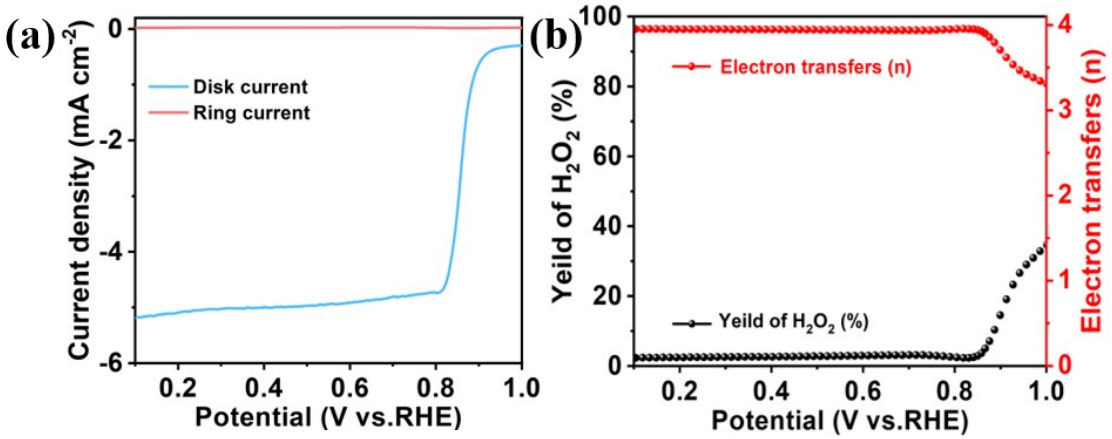

Fig. S7. (a) RRDE polarization curves for disk current and ring currents of FeCo/NC; (b) Plots of the ORR apparent electron transfer number (n) and H_2O_2 production (%) of FeCo/NC obtained from RRDE.

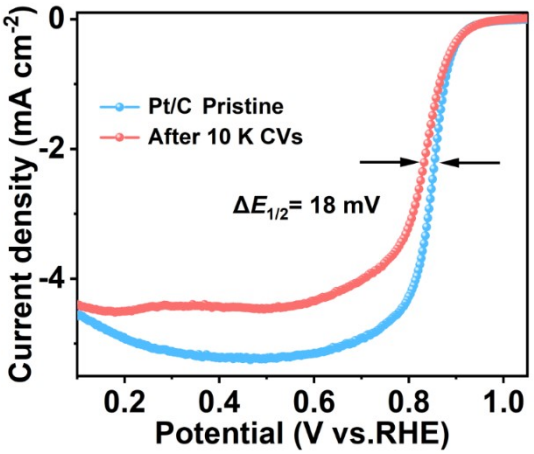

Fig. S8. Measurement of long-term operation durability of Pt/C (20 wt.%).

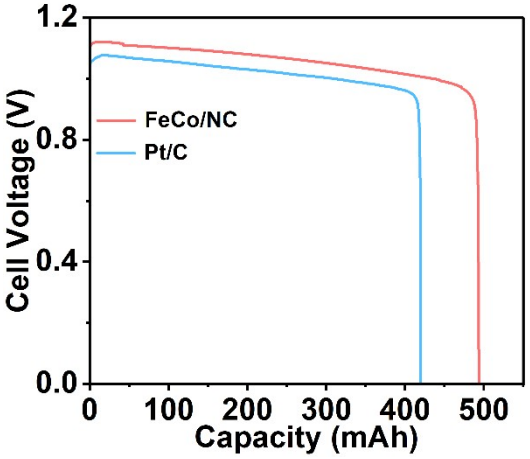

Fig. S9. The zinc–air battery measurement of FeCo/NC and Pt/C (20 wt.%) for discharge capacity.

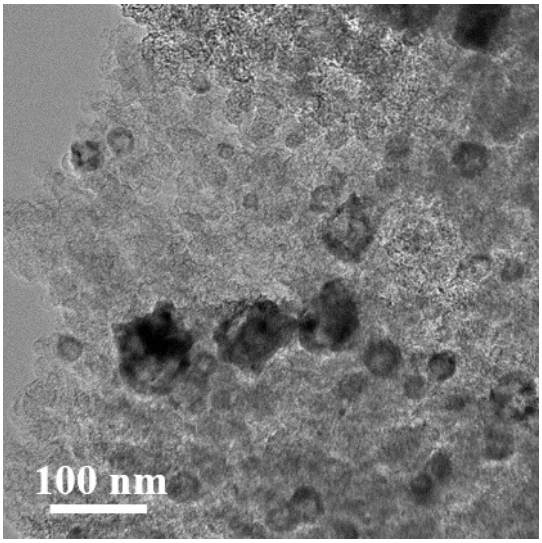

Fig. S10. Bright-field TEM image of FeCo/NC after 48 h of ZAB charge−discharge cycle.

Part III. Supplementary Tables

Table S1. Fe and Co content and the corresponding half-wave potentials ($E_{1/2}$) in the prepared catalyst. (Metal content in the prepared catalysts was detected using ICP-OES.)

Sample	Fe (wt.%)	Co (wt.%)	$E_{1/2}$ (V)
Fe/NC	0.52	/	0.815
Co/NC	/	3.05	0.806
FeCo/NC-800	0.51	3.09	0.831
FeCo/NC-900 (Denoted as FeCo/NC)	0.52	3.07	0.863
FeCo/NC-1000	0.54	3.10	0.852
20% Pt/C	/	/	0.850

Table S2. C, N, O, Fe and Co content obtained from XPS characterization in the corresponding catalyst.

Sample	C (at.%)	N (at.%)	O (at.%)	Fe		Co	
				at.%	wt.%	at.%	wt.%
Fe/NC	91.41	2.76	5.74	0.09	0.41	/	/
Co/NC	90.64	2.69	6.06	/	/	0.63	2.95
FeCo/NC	90.91	2.73	5.65	0.10	0.44	0.61	2.85

Table S3. N 1*s* peak position and proportion (%) of Pd-N, Pr-N, G-N and O-N in Fe/NC, Co/NC and FeCo/NC.

Sample		Pd-N	Pr-N	G-N	O-N
Fe/NC	Position (eV)	398.7	400.1	401.3	403.3
	Proportion (%)	43.4	32.1	15.1	9.4
Co/NC	Position (eV)	398.7	400.1	401.3	403.3
	Proportion (%)	42.5	29.8	17.1	10.6

FeCo/NC	Position (eV)	398.7	400.1	401.3	403.3
	Proportion (%)	47.6	28.6	14.3	9.5

Table S4. Fe 2*p* peak position of Fe^0 and Fe-N_x in Fe/NC and FeCo/NC.

Sample	Fe^0		Fe-N_x	
	$2p_{3/2}$	$2p_{1/2}$	$2p_{3/2}$	$2p_{1/2}$
Fe/NC	710.0	723.2	712.4	725.6
FeCo/NC	709.5	722.7	712.1	725.3

Table S5. Co 2*p* peak position of Co^0 and Co-N_x in Co/NC and FeCo/NC

Sample	Co^0		Co-N_x	
	$2p_{3/2}$	$2p_{1/2}$	$2p_{3/2}$	$2p_{1/2}$
Co/NC	780.0	794.9	782.1	796.7
FeCo/NC	780.2	795.1	782.1	796.7

Table S6. Quality of zinc sheet before and after discharge and the discharge capacity of FeCo/NC and Pt/C (20 wt.%).

Sample	Zinc sheet quality of before discharge (g)	Zinc sheet quality of after discharge (g)	Discharge capacity (mAh)
FeCo/NC	10.4607	9.8372	493.4
Pt/C(20 wt.%)	10.4280	9.7791	419.8

Table S7. The catalysts loading, specific capacity, power density, and long-life surface cycle of FeCo alloy-based catalysts in zinc-air batteries reported by previous work.

Catalyst	Catalyst loading (μg cm^{-2})	Specific capacity (mAh g^{-1} Zn)/Current density (mA cm^{-2})	Power density (mW cm^{-2})	Time (h)/ Current density (mA cm^{-2})	Ref.
FeCoNC/D	1000	725/10	157	40/10	(5)
Co_3Fe_7/CoC_x	1500	800/10	265	220/10	(8)
FeCo/N–CNTs-800	4000	763.53/10	200.4	445/10	(9)
FeCo-N-GCTSs	1000	/	133	288/5	(10)
FeCo-NC-60	/	703/10	132	/	(11)

$Fe_{0.2}Co_{0.8}$/N-C	/	807/10	159.1	550/10	(12)
FeCo/HP-NC	/	804.8/10	170.82	300/5	(13)
FeCo-NPCNs	1000	805.4 /10	161.2	400/10	(14)
FeCo/PCNs	1000	753.709/10	135	190/10	(15)
20 wt.%Pt/C	600	815.1/10	78.2	73/20	This work
FeCo/NC	1000	913.8/10	159.1	120/20	This work

Table S8. Chemicals used to prepare the corresponding FeCo alloy-based catalysts, number of major steps required for preparing the corresponding FeCo alloy-based catalysts, the morphology FeCo alloy nanoparticle (NP) and metal loading in the corresponding FeCo alloy-based catalysts.

Catalyst	Main chemicals	Number of synthesis steps[1]	Alloy morphology	Fe/Co loading	Ref.
FeCoNC/D	$FeCl_3·6H_2O$, $CoCl_2·6H_2O$, dicyandiamide ketjenblack,	~10	Irregular NP	0.8/1.19[2]	(5)
Co_3Fe_7/CoC_x	$Fe(NO_3)_3·9H_2O$, $Co(NO_3)_2·6H_2O$, melamine, cyanuric acid, tannic acid	~7	Irregular NP	14.8/2.8[3]	(8)
FeCo/N–CNTs-800	$FeCl_2·4H_2O$, $CoCl_2·6H_2O$, $(NH_4)_2S_2O_8$ NaOH	~8	Irregular NP	/	(9)
FeCo-N-GCTSs	melamine, $Fe(NO_3)_3·9H_2O$, $Co(NO_3)_2·6H_2O$, g-C_3N_4, 8-aminoquinoline	~7	Irregular NP	0.2/ 0.28[2]	(10)
FeCo-NC-60	$FeCl_3·6H_2O$, $Co(NO_3)_2·6H_2O$, 2-Methylimidazole	~12	Irregular NP	0.9/ 31.8[3]	(11)
$Fe_{0.2}Co_{0.8}$/N-C	$Fe(NO_3)_3·9H_2O$, $Co(NO_3)_2·6H_2O$, $Zn(NO_3)_2·6H_2O$, DMF, 2-Melm	~10	Irregular NP	0.64/ 1.68[2]	(12)
FeCo/HP-NC	$Fe(NO_3)_3·9H_2O$, $Co(NO_3)_2·6H_2O$, NaCl, glucose, urea	~7	Irregular NP	/	(13)
FeCo-PCNs	$FeCl_3·6H_2O$, $CoCl_2·6H_2O$, Fluorine-127, Dopamine, Mesitylene, hydrochloride dicyandiamide	~11	Irregular NP	3.15/5.22[3]	(14)
FeCo/NPCNs	$FeCl_3.6H_2O$, $CoCl_2.6H_2O$, terephthalic acid melamine, DMF	~10	Irregular NP	/	(15)
Co_3Fe_7/CNs-800	FePc, Fe_2O_3 CoPc, dicyandiamide	~6	Irregular NP	0.51/0.27[2]	(16)
FC@NCs	$Fe(NO_3)_3·9H_2O$, $C_4H_6CoO_4·4H_2O$, melamine, 2-methylimidazole, soya bean oil	~8	Irregular NP	10.9/44.0[3]	(17)
FeCo/NC	$FeCl_3$, CoO, melamine, Black Pearls	2	Circular trough-like NP	0.10/0.60[2] 0.52/3.07[3]	This work

[1]The main steps required for preparing FeCo alloy-based catalysts mainly include preparation and pretreatment of the supports, mixing and dispersion of chemical reagents, hydrothermal reaction, and heat treatment, acid treatment, washing and drying of solid powder, etc.
[2]The Fe/Co loading (at.%) in the corresponding catalysts was determined from XPS characterization results.
[3]The Fe/Co loading (wt.%) in the corresponding catalysts was determined from ICP test.

Part IV. Supplementary References

[S1] M. Xiao, et al., Adv. Mater., 2015, **27**, 2521–2527.
[S2] Y. Wang, et al., Angew. Chem. Int. Ed., 2023, **62**, e202219191.
[S3] H. Kim, et al., ChemElectroChem, 2019, **6**, 4757–4764.
[S4] X. Wen, et al., Chem. Eng. J., 2023, **454**, 140312.
[S5] K. Kim, et al., Appl. Catal., B., 2022, **315**, 121501.
[S6] J. Gamby, et al., J. Power Sources, 2001, **101**, 109-116.
[S7] G. Long, et al., Chinese. J. Catal. 2015**, 36**, 1197-1204.
[S8] L. Xiao, et al., J. Colloid Interface Sci., 2024, **655**, 427–438.
[S9] J. Chen, et al., Dalton Trans., 2022, **51**, 14498–14507.
[S10] L.-L. Liu, et al., J. Colloid Interface Sci., 2023, **639**, 424–433.
[S11] W. Li, et al., ACS Appl. Nano Mater., 2023, **7**, 27801–27810.
[S12] H. Huang, et al., Small, 2024, 2**0**, 2310318.
[S13] D. Sun, et al., ACS Appl. Nano Mater., 2024, **7**, 14760–14768.
[S14] Y. Lei, et al., Int. J. Hydrogen Energy, 2024, **65**, 437–444.
[S15] L. Lin, et al., J. Alloys Compd., 2022, **909**, 164625.
[S16] L. Wen, et al., J. Colloid Interface Sci., 2020, **569**, 277-285.
[S17] X. Luo, et al., J. Colloid Interface Sci., 2021, **590**, 622–631.